20th Australasian Fluid Mechanics Conference
Perth, Australia
5-8 December 2016

Turbulent characteristics produced by a blockage of pre-fractal emergent obstacles

J. E. Higham, W. Brevis and C. J. Keylock

Department of Civil & Structural Engineering
University of Sheffield, Sheffield, United Kingdom

Abstract

Stereo Particle Image Velocimetry (SPIV) measurements were undertaken to quantify the flow characteristics created by the blockage of a turbulent open channel by different sets of emergent obstacles, all with the same porosity. Four sets of obstacles were tested including an in-line regular sized obstacle, and three arrangements of multi-scale (pre-fractal) obstacles; one arranged as a Sierpinski carpet, and the other two ordered by obstacle size (i.e. large to small and vice versa). It is found that the pre-fractals create a protracted peak of turbulence intensity, when compared with a regular obstacle. Likewise, by rearranging the Sierpinski carpet it is possible to change the distribution of turbulence intensity. Using a Proper Orthogonal Decomposition further investigations are undertaken to determine the mechanisms underpinning the physics of these characteristics.

Introduction

The recent computational and experimental works of Hurst & Vassilicos (2007), Nicolle & Eames (2011), Laizet & Vassilicos (2011), Gomes-Fernandes et al. (2012), Laizet & Vassilicos (2015) have found pre-fractal grids to have a profound effect on the generation and control of turbulent wakes. Collectively these studies have shown the flow produced in the wake of a pre-fractal grid to be significantly different to that of a grid with a single length scale, of the same porosity. The multiple length scales associated to the mutliscale grids have been found to organise turbulent flows and create protracted regions of high turbulence intensity, making them ideal candidates for mixing applications.

In the present study an array of multiscale square cylinders are used to create a set of pre-fractal obstacles, and obstruct a turbulent flow. An investigation into the turbulent properties of the wake produced by these obstacles is undertaken using Stereo Particle Image Velocimetry (SPIV) measurments. Four experimental cases are chosen (see Fig. 1): The first an obstacle containing only a single length scale (Case I); the second an obstacle containing three length scales arranged in a 'Sierpinski Carpet' (Sierpinski 1916) (Case II); and the third and fourth two alternate arrangements of the 'Sierpinski Carpet' (Case III & IV). Each iteration within the pre-fractals is related by a scale factor of 3. All the obstacles extend the whole depth of the flow. The dimensions of the single square cylinder used in Case I is the same as the second iteration of the pre-fractal cases.

In an engineering context multi-scale obstacles can be found as vegetation blocking rivers. These in particular obstacles are chosen as they all have the same porosity; the three pre-fractal obstacles have the same 'fractal dimension' (Mandelbrot 1967); the two rearrangements have the same 'Lacunarity' (Mandelbrot 1990); and, all of the obstacles have the a different 'Succolarity' (de Melo & Conci 2013).

The present study is structured as follows: First, the mean streamwise velocities are presented; second the turbulent intensity created in the evolution of the wake is investigated; and finally, using a Proper Orthogonal Decomposition, the turbulent flow structures and their related energy contributions and dynamics are examined.

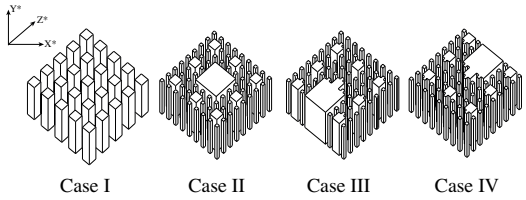

Figure 1: A three-dimensional representation of the different flow cases

Experimental Set-up

In a 0.5 m (width) $\times$ 18 m (length) open channel water flume at the University of Sheffield, UK, at a Reynolds number of Re=19,000 (where Re=$U_0 D/\mu$, U_0 is the inlet flow, D, is the hydraulic radius and μ is the kinematic viscosity) Stereo Particle Image Velocimetry measurements (SPIV) were undertaken along the centre line of the flow, parallel to the depth (see Fig. 2). The height of water was 0.3 m, and inlet flow was set to Q=0.10 l/s. The water flume has full optical access; the laser was mounted below with the cameras mounted perpendicular to the flows depth. Images were acquired using three Imager MX 4M cameras arranged around a glass prism to reduce optical distortion. The flow was seeded with 100 μm spherical 'Poylamid 12' particles and illuminated by a double pulsed Nd:YAG laser. The SPIV calculations were undertaken using the LaVision FlowMaster software. A multi-pass dynamic interrogation window was used ranging from 64px to 32px, with an overlap of 50%. For each experimental case 6 experimental planes were taken, each with an overlap of $\approx$ 10%. At each location 6,000 vector fields were captured at 25Hz. The centre of the images was located at the centre depth of the flow, as to not be affected by boundary effects. The size of each acquired image and result vector field was 130 mm $\times$ 100 mm. From the SPIV calculations three velocity components are determined: the streamwise velocity u, the vertical velocity v and the spanwise velocity, w. As the second iteration of the pre-fractals occurs in all of the experimental cases, a co-ordinate system is created and normalised by this dimension; where X^* is the streamwise direction, Y^* is the vertical dimension and Z^* is the spanwise dimension. The data was post processed using the PODDEM algorithm (Higham et al. in press)

Proper Orthogonal Decomposition

POD is a statistical method commonly used in fluid mechanics for the extraction and analysis of energy meaningful turbulent structures (Aubry 1991, Berkooz et al. 1993). POD was independently derived by a number of individuals, consequently acquiring a variety of names in different fields including Karhunen-Loève Decomposition, Singular Value Decomposition (SVD) and Principal Components Analysis (PCA) (Kosambi 1943, Loève 1945, Karhunen 1946, Pougachev 1953, Obukbov 1954). POD extracts energy relevant structures (modes) from set of a stochastic, statistically steady-state turbu-

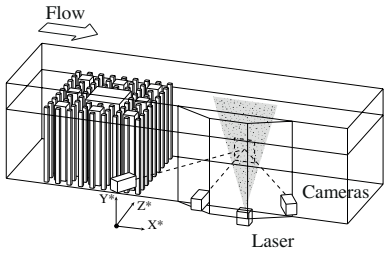

Figure 2: Experimental Set-up

lent fields, within a finite time domain, ordering them by their contribution to the total variance of the physical property being analysed, e.g. velocity (Brevis & García-Villalba 2011). A set of $t = 1,2,\ldots,T$ temporally ordered vector fields,$\mathbf{V}(x,y;t)$, is considered, each of which is of size $X \times Y$. The method requires the construction of a $N \times T$ matrix $\mathbf{W}$ from T columns $\mathbf{w}(t)$ of length $N = XY$, each column corresponding to a column-vector version of a transformed snapshot $\mathbf{V}(x,y;t)$. A POD can be obtained as the solution of a SVD:

$$\mathbf{W} \equiv \mathbf{PSC}^{\mathrm{T}} \tag{1}$$

where $\mathbf{S}$ is a matrix of size $\Omega \times \Omega$, (Ω are the number of modes of the decomposition, and $(\cdot)^T$ represents a transpose matrix operation). The $\lambda = \mathrm{diag}(\mathbf{S})^2/(N-1)$ is the vector containing the contribution to the total variance of each Ω. The elements in λ are ordered in descending rank order, i.e. ($\lambda_1 \geq \lambda_2 \geq \ldots \lambda_\Omega \geq 0$). In practical terms the matrix $\mathbf{P}$ of size $N \times \Omega$ contains the spatial structure of each of the modes and the matrix $\mathbf{C}$ of size $\Omega \times \Omega$ contains the coefficients representing the time evolution of the modes.

Results

Figure 3 presents the mean streamwise velocity, in Case I, as expected, there is a negative region of streamwise velocity in the near wake of the obstacle at X* =1–2. Out of all of the cases, this case regains a steady streamwise velocity in the shortest streamwise distance. In all of the pre-fractal cases a similar negative region of velocity is observed. Interestingly this region occurs at the same location X* =2–4, although the magnitude and distribution of this region differs corresponding to the arrangement. Out of the three pre-fractal cases, it is found the rate of change in the direction of velocity from back from negative to positive, in Case II is smallest. Out of all of the cases it is found that Case IV produces the greatest change in velocity magnitude. Unlike Case II, Cases III & IV regain a steady streamwise velocity at a much shorter streamwise distance.

In Fig. 4 the turbulence intensity $\mathbf{u}'/U_0$, i.e. the root-mean-square of the velocity fluctuations at 40% of the flows depth is presented. Fig. 4 (a) shows the turbulence intensity plotted against X*. The figure shows the peak turbulent intensity for Case I is located after the intense change in direction of the streamwise velocity (X*=2). Likewise, in all of the pre-fractal cases the peak turbulence intensity occurs at the same location, relating to the similar event (X*=4). In Fig. 4 (b) the streamwise distance is normalised by the location of the peak turbulence intensity x^{peak}. This figure highlights that in the pre-fractal cases the growth and decay of the turbulence intensity is dependent on the arrangement. In Case II the growth and decay of the turbulence intensity is smooth with no additional peaks, resembling and elongated stretched Case I. In Case III, where the largest iteration is located at the back of the fractal a deficit is seen in the growth region and as a consequence the turbulence intensity decays at a slower rate. In Case IV, where the largest iteration is

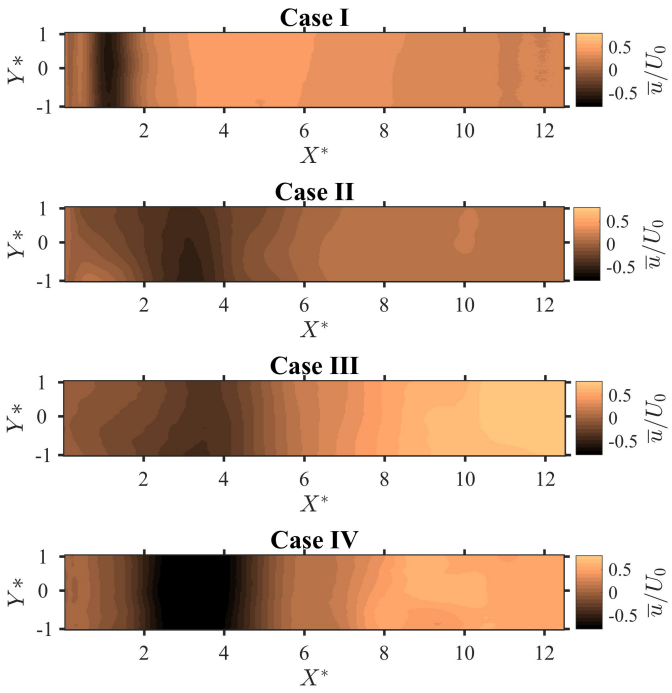

Figure 3: Mean streamwise velocities for each case normalised by inlet velocity U_0

located at the front of the obstacle, a secondary peak is observed in the production region, the presence of which may explain enhanced rate of decay.

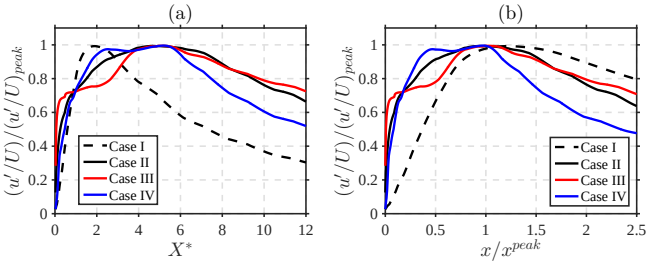

Figure 4: Turbulence intensity, $\mathbf{u}'/U_0$, plotted against the streamwise distance in: (a) The streamwise distance is normalised by the second iteration; (b) the streamwise distance is normalised by the location of the peak turbulence intensity (x^{peak}).

Proper Orthogonal Decomposition

A POD is computed from all 6,000 velocity fields using all three components. In the present study the streamwise modes are presented. For a POD synchronous vector fields are required. As a result multiple computations are undertaken for each case.

From an general overview of all the POD spatial modes it appears that in the top two modes, between each case the large scale spatial structures are similar. However, between Case I and the pre-fractal cases it is apparent that there is a change in order of the distribution of the spatial modes; suggesting the pre-fractal geometries are causing a redistribution of the turbulent kinetic energy of the large scale turbulent structures within the wake. To investigate this further the variance of the top two modes, as determined in λ, is presented in Fig. 6 as a percentage of the mean flow. From this figure it is evident that even

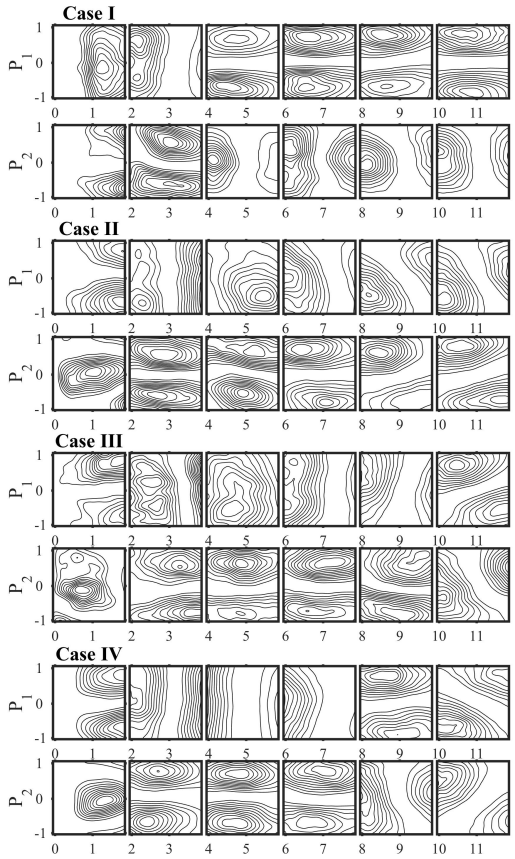

Figure 5: Top two leading spatial modes, $\mathbf{P}_1$ and $\mathbf{P}_2$, computed from a POD. Only the streamwise component of the decomposition is presented.

though spatially the top two POD modes resemble one another in the pre-fractal cases they contain a far greater contribution of the total variance i.e. turbulent kinetic energy. This is especially evident between $X^* = 4$–6, i.e. the location of the peak turbulent intensity.

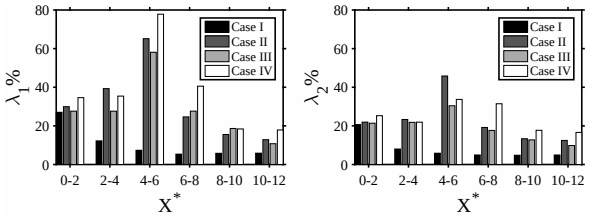

Figure 6: The percentage of the variance of the flow λ calculated for each POD calculation, with respect to the mean.

To investigate the dynamical behaviour of these large scale structures a power density spectrum of the temporal coefficients of the top two modes of $\mathbf{C}$ is calculated using Welch's implementation Welch (1967) of the fast Fourier transform. The frequency is expressed as a function of the Strouhal number defined as $St = f/LU_0$, where f is the frequency and L is the dimension of the second iteration square cylinder. At first glance it is apparent that spatial structures are complex and contain many different turbulent length scales. On closer inspection it is evident within these complex distributions there are a number of dominant frequencies. As shown in Fig. 6 in the first and second plane of Case I, in the leading mode (black line) a peak frequency at St=1.3 occurs. This frequency is likely to be associated to turbulent interactions produced from the flow structures shed from the cylinders. In the second mode (red line) further downstream in the fourth plane a second frequency is observed, at St=0.58. This position relates to X^*=6–7 which from the spatial modes relates to the formation of a large scale coherent structure. In all of the pre-fractal cases, at differing locations, in the top two leading modes two frequencies are observed; St=0.25 and again St=0.58. These two frequencies are especially prominent in case III. It is therefore hypothesised that these frequencies relate to the shedding of turbulent structures from different iterations of obstacles, and each fractal iteration has its own specific signature within the wake. Whilst there are modal decomposition techniques which allow the extraction of such structures this is beyond the scope of this conference paper and will be the subject of further work.

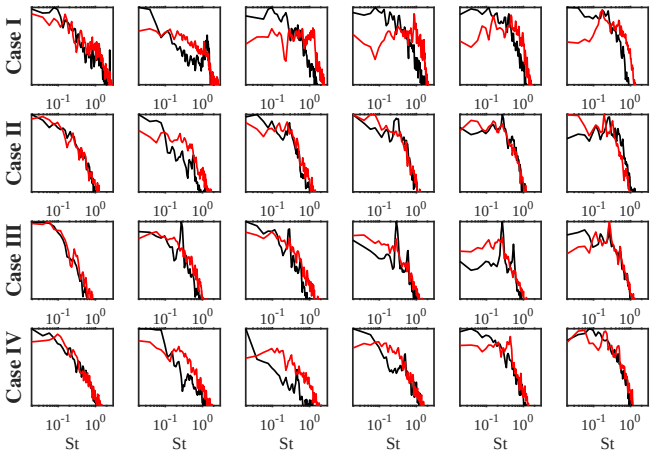

Figure 7: Fourier Spectra taken of the temporal coefficients relating to top two POD modes, plotted against Strouhal number - black and red lines relate to $\mathbf{C}_1$ and $\mathbf{C}_2$ respectively.

Conclusions

From these preliminary investigations, it is determined that the turbulent wake created by a pre-fractal multiscale obstacle is significantly different to that created by an obstacle with only a single length scale, and the same porosity. It is found that pre-fractals obstacles create a protracted region of turbulence intensity, the growth and decay rate of which can be chnaged by arranging the fractal in a different manner. From a POD analysis it is determined that similar large scale turbulent structures are produced in the wake of all of all the obstacles, however those in the wake of the pre-fractals have a different energy distribution. Further investigations in to the POD spectra provide evidence that each of the pre-fractals iterations creates its own signature within the turbulent wake. Concluding further work is require to investigate how these signatures propagate within the wake, what is their effect on the growth and decay of turbulence intensity and how changing a fractals arrangement alters the iterations signature.

Acknowledgements

The UK Natural Environment Research Council for the support to the first author and Engineering and Physical Sciences Research Council for the second author.

*

References

Aubry, N. (1991), 'On the hidden beauty of the proper orthog-

onal decomposition', *Theoretical and Computational Fluid Dynamics* **2**(5-6), 339–352.

Berkooz, G., Holmes, P. & Lumley, J. L. (1993), 'The Proper Orthogonal Decomposition in the analysis of turbulent flows', *Annual Review Fluid Mechanics* **25**(1), 539–575.

Brevis, W. & García-Villalba, M. (2011), 'Shallow-flow visualization analysis by Proper Orthogonal Decomposition', *Journal of Hydraulic Research* **49**(5), 586–594.

de Melo, R. H. & Conci, A. (2013), 'How succolarity could be used as another fractal measure in image analysis', *Telecommunication Systems* **52**(3), 1643–1655.

Gomes-Fernandes, R., Ganapathisubramani, B. & Vassilicos, J. (2012), 'Particle image velocimetry study of fractal-generated turbulence', *Journal of Fluid Mechanics* **711**, 306–336.

Higham, J., Brevis, W. & Keylock, C. (in press), 'A rapid non-iterative proper orthogonal decomposition based outlier detection and correction for PIV data', *Measurments Science and Technology* .

Hurst, D. & Vassilicos, J. (2007), 'Scalings and decay of fractal-generated turbulence', *Physics of Fluids (1994-present)* **19**(3), 035103.

Karhunen, K. (1946), 'Zur spektral theorie stochastischer prozesse', *Annales Academiæ Scientiarum Fennicæ* **A1:34**.

Kosambi, D. (1943), 'Statistics in function space', *Journal of Indian Mathematical Society* **7**, 76–88.

Laizet, S. & Vassilicos, J. (2015), 'Stirring and scalar transfer by grid-generated turbulence in the presence of a mean scalar gradient', *Journal of Fluid Mechanics* **764**, 52–75.

Laizet, S. & Vassilicos, J. C. (2011), 'Dns of fractal-generated turbulence', *Flow, turbulence and combustion* **87**(4), 673–705.

Loève, M. (1945), 'Functions aleatoire de second ordre.', *Comptes Rendus de l'Académie des Sciences* **220**.

Mandelbrot, B. (1990), 'Fractals: a geometry of nature: fractal goemetry is the key to understanding chaos. it is also the geometry of mountains, clouds and galaxies', *New Scientist* **127**(1734), 38–43.

Mandelbrot, B. B. (1967), 'How long is the coast of britain', *Science* **156**(3775), 636–638.

Nicolle, A. & Eames, I. (2011), 'Numerical study of flow through and around a circular array of cylinders', *Journal of Fluid Mechanics* **679**, 1–31.

Obukbov, A. M. (1954), 'Statistical description of continuous fields.', *Trudy Geofizicheskogo Instituta, Akademiya Nauk SSSR* **24**, 3–42.

Pougachev, V. S. (1953), 'General theory of the correlations of random functions.', *Izvestiya Akademii Nauk SSSR. Seriya Matematicheskaya. Bulletin de l'Académie des Sciences de l'URSS* .

Sierpinski, W. (1916), 'Sur une courbe cantorienne qui contient une image biunivoque et continue de toute courbe donnée', *Comptes Rendus* **629**.

Welch, P. D. (1967), 'The use of fast fourier transform for the estimation of power spectra: A method based on time averaging over short, modified periodograms', *IEEE Transactions on audio and electroacoustics* **15**(2), 70–73.